YZβ discontinuity capturing for advection-dominated processes with application to arterial drug delivery

Y. Bazilevs[1,*,†,‡], V. M. Calo[1,‡], T. E. Tezduyar[2,§] and T. J. R. Hughes[1,¶]

[1]*Institute for Computational Engineering and Sciences, The University of Texas at Austin, 201 East 24th Street, 1 University Station C0200, Austin, TX 78712, U.S.A.*
[2]*Mechanical Engineering, Rice University, MS 321, 6100 Main Street, Houston, TX 77005, U.S.A.*

SUMMARY

The *YZβ* discontinuity-capturing operator, recently introduced in (*Encyclopedia of Computational Mechanics*, *Vol. 3*, *Fluids*. Wiley: New York, 2004) in the context of compressible flows, is applied to a time-dependent, scalar advection–diffusion equation with the purpose of modelling drug delivery processes in blood vessels. The formulation is recast in a residual-based form, which reduces to the previously proposed formulation in the limit of zero diffusion and source term. The NURBS-based isogeometric analysis method, proposed by Hughes *et al.* (*Comput. Methods Appl. Mech. Eng.* 2005; **194**:4135–4195), was used for the numerical tests. Effects of various parameters in the definition of the *YZβ* operator are examined on a model problem and the better performer is singled out. While for low-order B-spline functions discontinuity capturing is necessary to improve solution quality, we find that high-order, high-continuity B-spline discretizations produce sharp, nearly monotone layers without the aid of discontinuity capturing. Finally, we successfully apply the *YZβ* approach to the simulation of drug delivery in patient-specific coronary arteries. Copyright © 2007 John Wiley & Sons, Ltd.

*Correspondence to: Y. Bazilevs, Institute for Computational Engineering and Sciences, The University of Texas at Austin, 201 East 24th Street, 1 University Station C0200, Austin, TX 78712, U.S.A.
†E-mail: bazily@ices.utexas.edu
‡Postdoctoral Fellow.
§James F. Barbour Professor of Mechanical Engineering and Materials Sciences.
¶Professor of Aerospace Engineering and Engineering Mechanics, Computational and Applied Mathematics Chair III.

WILEY InterScience®
DISCOVER SOMETHING GREAT

1. INTRODUCTION

In order to treat coronary artery disease, it has been proposed to deliver drugs to the diseased region of the arterial wall. One such method of delivery is direct injection of the drug into the blood stream in hope that it would reach and penetrate into the arterial wall at a desired location. In order to make the procedure effective, that is, to deliver the necessary amount of the drug to the region of interest with minimal interference with the vascular system, one needs to optimize quantities such as the location of the injector, the injection rate, and the angle of injection. These optimizations can be performed by employing numerical simulation.

A simplified mathematical model that describes the behaviour of the drug in the blood stream is a time-dependent, scalar advection–diffusion equation. The scalar in the formulation represents the drug concentration in the blood. The advective velocity for the scalar is assumed to be the blood velocity. In this work we model the blood as an incompressible Newtonian fluid. It is also assumed that the drug concentration does not influence the flow physics. As a result, we have a one-way coupling, in which we first solve for the blood velocity and pressure, and then use the flow field to obtain the drug concentration. Drug dispersivity is assumed very small (yet non-negligible), implying that advective processes take place on a much faster time scale than drug dispersion. It needs to be emphasized that in the advective–diffusive model employed herein the drug cannot reach the wall without dispersion.

With the above assumptions, the transport equation models nearly pure advection phenomena that, for practical meshes, leads to unresolved interior and boundary layers, which, in turn, pose a challenge for most existing numerical techniques. Oscillations are typically seen in the vicinities of the layers. It is generally accepted that SUPG stabilization (see [1]) is not sufficiently dissipative in the vicinity of sharp gradients to preclude significant undershoots and overshoots in the discrete solution. Discontinuity capturing, also referred to as shock capturing, provides further dissipation and improves the quality of the discrete solution near sharp layers. Discontinuity-capturing operators are designed to be active in the region of high solution gradients and vanish quickly in the parts of the domain where the solution is smooth.

The paper is outlined as follows. In Section 2, we describe the strong and weak formulations of the continuous advection–diffusion problem and then formulate it at the discrete level. We employ SUPG stabilization augmented by a $YZ\beta$ discontinuity-capturing operator, which was originally proposed by Tezduyar [2] in the context of compressible flows, and was shown in [3–5] to produce results superior to existing formulations. We extend the original $YZ\beta$ definition to the scalar advection–diffusion case and rewrite it in the residual-based form. The rest of the paper is devoted to various numerical test cases. In all examples spatial discretization makes use of the NURBS-based isogeometric analysis approach (see [6–8]). Time integration is performed using the generalized-α method (see [9, 10]).

In Section 3, we consider a numerical example that deals with advection of an L-shaped discontinuity front. We focus on the performance of the method in the transient regime and compare solutions with and without discontinuity capturing. We also investigate the effects of the 'advective' *versus* the residual-based forms of the $YZ\beta$ operator. For second-order, C^1-continuous B-spline discretization we find that residual-based formulations produce sharper discontinuities without significant over- and under-shooting, and are less sensitive to the variations of the sharpness parameter β used in the definition of $YZ\beta$. By solving the same problem on the mesh of sixth-order B-splines that are C^5-continuous, we also find that high-order, high-continuity discretizations produce excellent quality layers without the aid of discontinuity capturing. This result confirms

the findings of Hughes *et al.* [8] for steady advection–diffusion problems. In Section 4, we apply the *YZβ* formulation of the advection–diffusion equation to model drug delivery in patient-specific coronary arteries. Second-order NURBS are employed in this example (for details of patient-specific NURBS geometry construction for use in isogeometric analysis, see [11]). In Section 5 we draw conclusions and outline future research directions.

2. ADVECTION–DIFFUSION EQUATION

2.1. Strong and weak formulations of the continuous problem

Let Ω be an open, connected, bounded subset of $\mathbb{R}^d$, $d = 2$ or 3, with piecewise smooth boundary $\Gamma = \partial\Omega$. Ω represents the fixed spatial domain of the problem. Let $f : \Omega \to \mathbb{R}$ be the given source; $\mathbf{a} : \Omega \to \mathbb{R}^d$ is the spatially varying velocity vector, assumed solenoidal; and $\boldsymbol{\kappa} : \Omega \to \mathbb{R}^{d \times d}$ is the diffusivity tensor, assumed symmetric, positive definite. The boundary value problem consists of solving the following equations for $\phi : \overline{\Omega} \to \mathbb{R}$:

$$\mathscr{L}\phi = f \quad \text{in } \Omega \tag{1}$$

$$\phi = g \quad \text{on } \Gamma_D \tag{2}$$

$$\boldsymbol{\kappa}\nabla\phi \cdot \mathbf{n} = h \quad \text{on } \Gamma_N \tag{3}$$

where

$$\mathscr{L}\phi = \frac{\partial \phi}{\partial t} + \mathbf{a} \cdot \nabla\phi - \nabla \cdot (\boldsymbol{\kappa}\nabla\phi) \tag{4}$$

and $g : \Gamma_D \to \mathbb{R}$ is the prescribed Dirichlet boundary data, $h : \Gamma_N \to \mathbb{R}$ is the prescribed Neumann boundary data, $\mathbf{n}$ is the unit outward boundary normal, $\Gamma = \Gamma_D \cup \Gamma_N$, and $\Gamma_D \cap \Gamma_N = \emptyset$.

Defining the solution and the weighting function spaces as

$$H_g^1(\Omega) = \{\phi \mid \phi \in H^1(\Omega), \ \phi = g \text{ on } \Gamma\} \tag{5}$$

$$H_0^1(\Omega) = \{\phi \mid \phi \in H^1(\Omega), \ \phi = 0 \text{ on } \Gamma\} \tag{6}$$

respectively, the variational counterpart of (1) reads: find $\phi \in H_g^1(\Omega)$ such that $\forall w \in H_0^1(\Omega)$,

$$\left(w, \frac{\partial \phi}{\partial t} + \mathbf{a} \cdot \nabla\phi\right)_\Omega + (\nabla w, \boldsymbol{\kappa}\nabla\phi)_\Omega = (w, f)_\Omega + (w, h)_{\Gamma_N} \tag{7}$$

where $(\cdot, \cdot)_A$ denotes the L^2-inner product on $A = \{\Omega, \Gamma\}$.

2.2. Discrete formulation and discontinuity capturing

Let $\mathscr{V}_g^h$ and $\mathscr{V}_0^h$ be the finite-dimensional spaces of trial solutions and weighting functions, respectively, where, as in the continuous case, subscripts g and 0 refer to essential boundary conditions. We state the semi-discrete formulation of the advection–diffusion problem as follows:

find $\phi^h \in \mathscr{V}_g^h$ such that $\forall w^h \in \mathscr{V}_0^h$,

$$
\left(w^h, \frac{\partial \phi^h}{\partial t} + \mathbf{a} \cdot \nabla \phi^h \right)_\Omega + (\nabla w^h, \boldsymbol{\kappa} \nabla \phi^h)_\Omega - (w^h, f)_\Omega - (w^h, h)_{\Gamma_\mathrm{N}}
$$

$$
+ \sum_{e=1}^{n_{el}} (\mathbf{a} \cdot \nabla w^h \tau, \mathscr{L} \phi^h - f)_{\Omega_e} + (\nabla w^h, \boldsymbol{\kappa}_\mathrm{dc} \nabla \phi^h)_{\Omega_e} = 0 \tag{8}
$$

In this work we make use of the spaces of NURBS functions employed in isogeometric analysis [8]. The developments that follow are equally applicable to standard finite element discretizations. The above formulation of advection–diffusion makes use of SUPG stabilization, in which

$$
\tau = \frac{h_\mathbf{a}}{2|\mathbf{a}|} \min \left(1, \frac{1}{3 p^2} Pe \right) \tag{9}
$$

where *Pe*, the element Peclet number, is defined as

$$
Pe = \frac{|\mathbf{a}| h_\mathbf{a}}{2|\boldsymbol{\kappa}|} \tag{10}
$$

$h_\mathbf{a}$ is the element size in the direction of the flow, and p is the polynomial order of the basis. For a summary of the early literature on the SUPG formulation, see Brooks and Hughes [1]. Recent work on stabilized methods is presented in [12–25]. The definition of the intrinsic time scale τ, given by (9), is adequate for simple element geometries. It is based on a single, advective length scale, $h_\mathbf{a}$. A more general definition, which involves a second, diffusive length scale, is given and utilized in the description of the drug delivery computations. Other definitions of τ based on multiple length scales are presented in [24, 25]. The last term of (8) is the discontinuity-capturing operator, and $\boldsymbol{\kappa}_\mathrm{dc}$ is the associated diffusivity tensor. We make use of the so-called $YZ\beta$ definition of $\boldsymbol{\kappa}_\mathrm{dc}$ introduced in [2] for compressible flows. In this work we start by extending that formulation to the unsteady, scalar advection–diffusion equation.

The discontinuity-capturing diffusion tensor $\boldsymbol{\kappa}_\mathrm{dc}$ is defined as

$$
\boldsymbol{\kappa}_\mathrm{dc} = \kappa_\mathrm{dc} \mathbf{D} \tag{11}
$$

where κ_dc is the magnitude and $\mathbf{D}$ defines the direction in which the operator is applied. When $\mathbf{D} = \mathbf{I}$, the identity tensor, the discontinuity-capturing diffusion is isotropic. Extending the definition of κ_dc given in [2, 25] to the scalar case, we get

$$
\kappa_\mathrm{dc} = |Y^{-1} Z| \left(\sum_{i=1}^{d} \left| Y^{-1} \frac{\partial \phi^h}{\partial x_i} \right|^2 \right)^{\beta/2 - 1} \left(\frac{h_\mathrm{dc}}{2} \right)^\beta \tag{12}
$$

where

$$
Y = \phi_\mathrm{ref} \tag{13}
$$

is the reference value of the scalar field ϕ^h, and

$$
h_\mathrm{dc} = 2 \left(\sum_{a=1}^{n_{shl}} |\mathbf{j} \cdot \nabla N_a| \right)^{-1} \tag{14}
$$

is the local element length scale. In (14), $\mathbf{j} = \nabla\phi^h / \|\nabla\phi^h\|$, N_a is the element basis function, and n_{shl} is the total number of element basis functions. The parameter β in (12) influences the smoothness of the layer. For smoother layers it is set to 1, while for sharper layers it set to 2.

The original *YZβ* is defined in [2, 25] as

$$Z = \mathbf{a} \cdot \nabla\phi^h \tag{15}$$

or

$$Z = \frac{\partial \phi^h}{\partial t} + \mathbf{a} \cdot \nabla\phi^h \tag{16}$$

Expression (15) is applicable to the steady case, while (16) is to be used for time-dependent problems. Note that the original definition is not consistent, namely it does not vanish on the exact solution. In view of this we propose to modify the definition of Z to

$$Z = \mathscr{L}\phi^h - f \tag{17}$$

In the absence of the source term, and because one typically employs discontinuity capturing for very small or zero physical diffusion, definition (17) reduces to (15) for the steady problem, and to (16) for the time-dependent case.

In our case, where time-dependent behaviour is of interest and diffusion is very small, formulations employing (17) and (16) are, for all practical purposes, equivalent. Numerical examples presented in the next section indicate that omitting the time-derivative term from the definition of Z for time-dependent problems leads to discontinuities that are overly diffuse. This is an important observation, as the computations reported in [3–5] were steady-state computations, and, as a result, employed (15). Furthermore, our numerical experiments show that the choice of the Z term has greater influence on the sharpness of the discontinuity than the parameter β.

3. TESTS WITH AN L-SHAPED DISCONTINUITY ADVECTED SKEW TO MESH

The problem set-up is given in Figure 1. The scalar diffusivity $\boldsymbol{\kappa}$ is assumed isotropic, that is $\boldsymbol{\kappa} = \kappa \mathbf{I}$ with $\kappa = 10^{-6}$. The angle of advection is chosen to be $45°$ and the magnitude of the advective speed is set to unity. The domain is a unit square subdivided into 20×20 square elements. At time $t = 0$ the value of the scalar field is set to unity in the interior of the L-shaped block located in the lower left-hand corner of the domain. Elsewhere in the domain ϕ^h is set to zero, creating an interior layer with an L-shaped concave front. We chose this initial shape in order to demonstrate robustness and accuracy of the method, since advecting concave surfaces is more challenging than convex ones. The solution is advanced in time until $t = 0.25$. Given that the diffusion coefficient is very small compared to the advection velocity and the mesh size, for all practical purposes the problem corresponds to pure advection. We will refer to the interior layer as the discontinuity front, and its location and shape at the final time ($t = 0.25$) are illustrated in Figure 1 with dashed lines.

Figures 2–4 present results for second-order, C^1-continuous NURBS (B-splines in this case due to the simple geometry). We investigate the *YZβ* discontinuity-capturing operator and test advective ($Z = \mathbf{a} \cdot \nabla\phi^h$) *versus* residual-based ($Z = \mathscr{L}\phi^h - f$) formulations, as well as parameter values $\beta = 1$ and 2. We compare simulation results at $t = 0.25$ in order to examine the ability of a given discrete
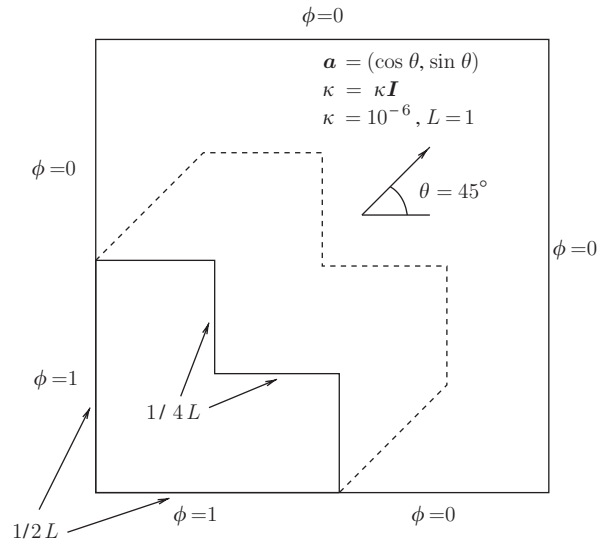
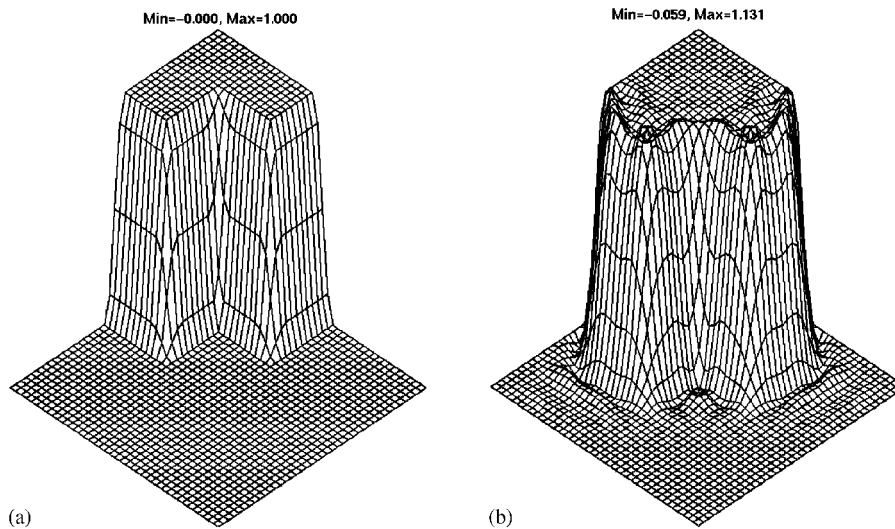Figure 1. Advection of an L-shaped front. Problem description.

Figure 2. Advection of an L-shaped front. Results using C^1-continuous quadratic splines. Elevation plot of the solution interpolated with 40×40 bilinear elements: (a) initial condition and (b) SUPG without discontinuity capturing.

formulation to generate time-dependent solutions that preserve the sharpness of the discontinuities without excessive undershooting and overshooting. We first note that advective formulations produce significantly more smeared shocks than their residual-based counterparts. We also observe that in the case of the residual-based method the sharpness of the discontinuity is not as strongly
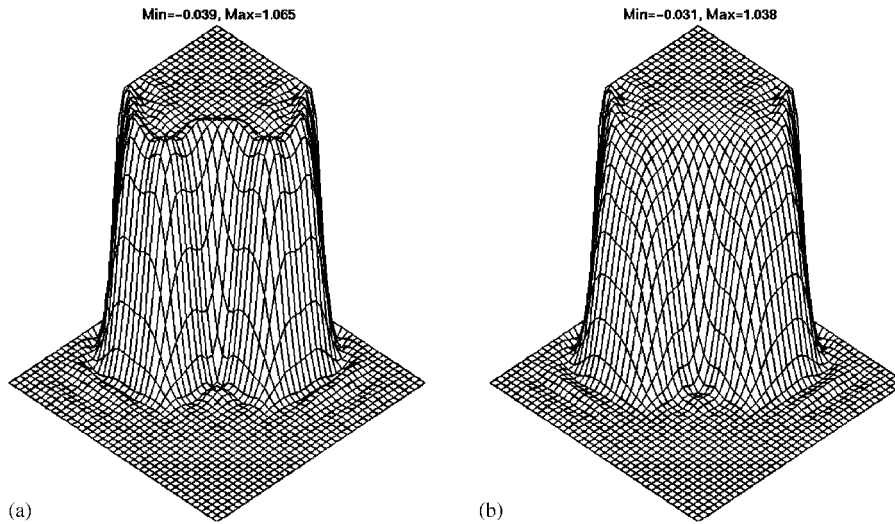
Min=−0.039, Max=1.065   Min=−0.031, Max=1.038

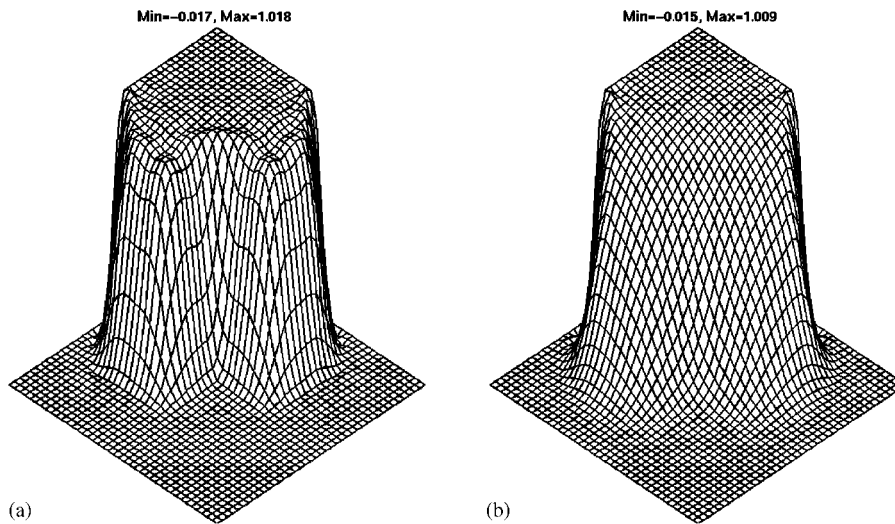(a)   (b)

Figure 3. Advection of an L-shaped front with discontinuity capturing. Results using C^1-continuous quadratic splines. Elevation plot of the solution interpolated with 40×40 bilinear elements: (a) residual-based ($Z = \mathscr{L}\phi^h - f$), $\beta = 2$ and (b) advective ($Z = \mathbf{a} \cdot \nabla\phi^h$), $\beta = 2$.

Min=−0.017, Max=1.018   Min=−0.015, Max=1.009

(a)   (b)

Figure 4. Advection of an L-shaped front with discontinuity capturing. Results using C^1-continuous quadratic splines. Elevation plot of the solution interpolated with 40×40 bilinear elements: (a) residual-based ($Z = \mathscr{L}\phi^h - f$), $\beta = 1$ and (b) advective ($Z = \mathbf{a} \cdot \nabla\phi^h$), $\beta = 1$.

dependent on β as for the advective case. Finally, we conclude that for this level of discretization the combination of residual-based formulation and $\beta = 1$ appears to be most favourable.

The next set of results makes use of C^5-continuous B-splines of degree six on the same mesh. It was demonstrated on a particular problem in Hughes *et al.* [8] that high-order, high-continuity
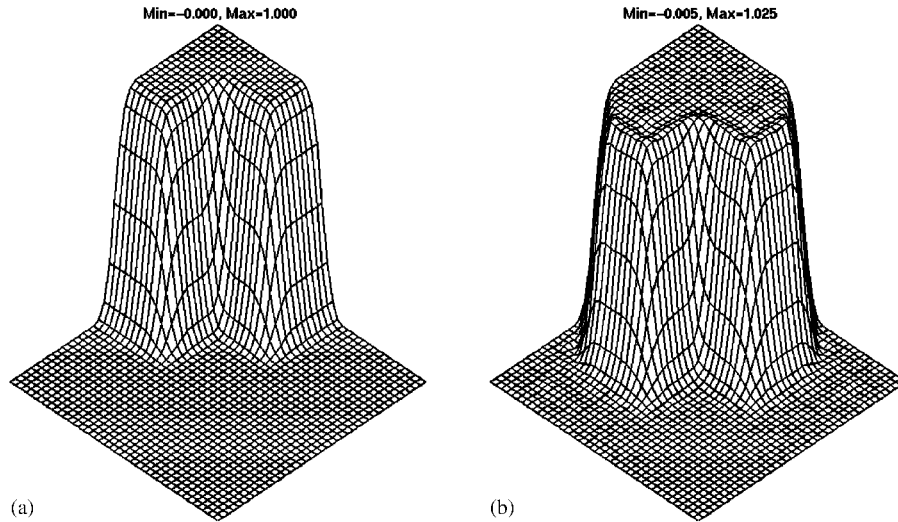
Min=−0.000, Max=1.000   Min=−0.005, Max=1.025

(a)   (b)

Figure 5. Advection of an L-shaped front. Results using C^5-continuous splines of order six. Elevation plot of the solution interpolated with 40×40 bilinear elements. Note the sharpness and lack of significant undershoots and overshoots in the SUPG solution without discontinuity capturing: (a) initial condition and (b) SUPG without discontinuity-capturing.
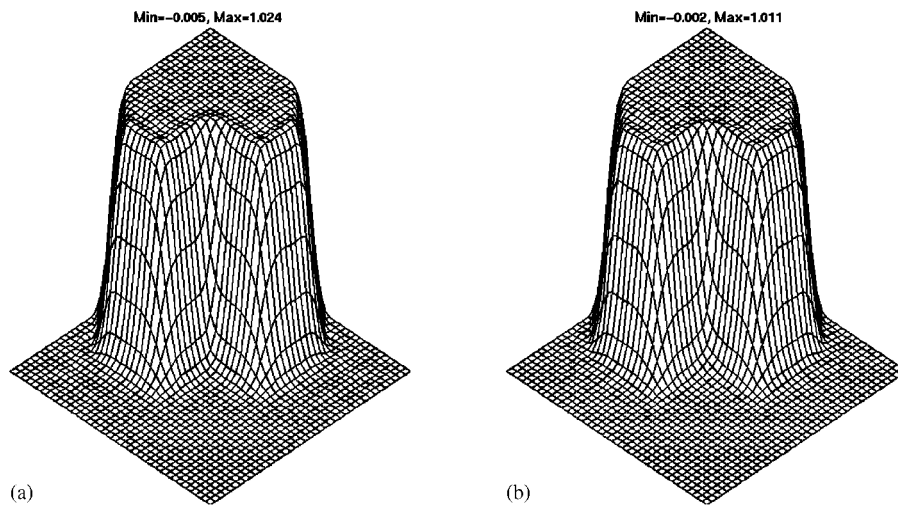
Min=−0.005, Max=1.024   Min=−0.002, Max=1.011

(a)   (b)

Figure 6. Advection of an L-shaped front with discontinuity capturing. Results using C^5-continuous splines of order six. Elevation plot of the solution interpolated with 40×40 bilinear elements: (a) residual-based $(Z = \mathscr{L}\phi^h - f)$, $\beta = 2$ and (b) residual-based $(Z = \mathscr{L}\phi^h - f)$, $\beta = 1$.

discretizations in conjunction with a *linear* stabilized method converge to monotone solutions in the presence of thin layers for steady advection–diffusion. Results of this computation, shown in Figures 5 and 6, indicate that the same behaviour is observed for time-dependent advection–

diffusion cases. Furthermore, only a slight improvement in the $p = 6$ solution is achieved by using the discontinuity-capturing operator.

It should be noted that boundary conditions for both $p = 2$ and 6 were set according to the technique described in [8] in which the control variables interpolate the prescribed data. Since the B-spline spaces are non-nested for various polynomial orders, the boundary conditions are slightly different for both cases, the $p = 6$ case being somewhat more smeared due to the greater support of the basis functions (see Figures 2(a) and 5(a) for a comparison).

4. PATIENT-SPECIFIC MODELLING OF DRUG DELIVERY IN CORONARY ARTERIES

In this computational study we have developed a model, which makes use of patient-specific geometry of a portion of the coronary arterial tree of a healthy over 55 volunteer obtained from 64-slice CT angiography. The set-up for this study is illustrated in Figure 7. At the inlet of the artery we have placed a nearly cylindrical catheter for the purpose of injecting the drug into the blood stream. Blood is described as an incompressible Newtonian fluid with density of $1.06 \, \text{g/cm}^3$ and viscosity of $0.035 \, \text{g/(cm s)}$. A periodic flow waveform is applied at the inlet with a period of 1 s. The catheter is assumed to inject the drug into the flow at the speed of 4 cm/s in the direction normal to its lateral surface. It is also assumed that the drug is injected from the bottom half of
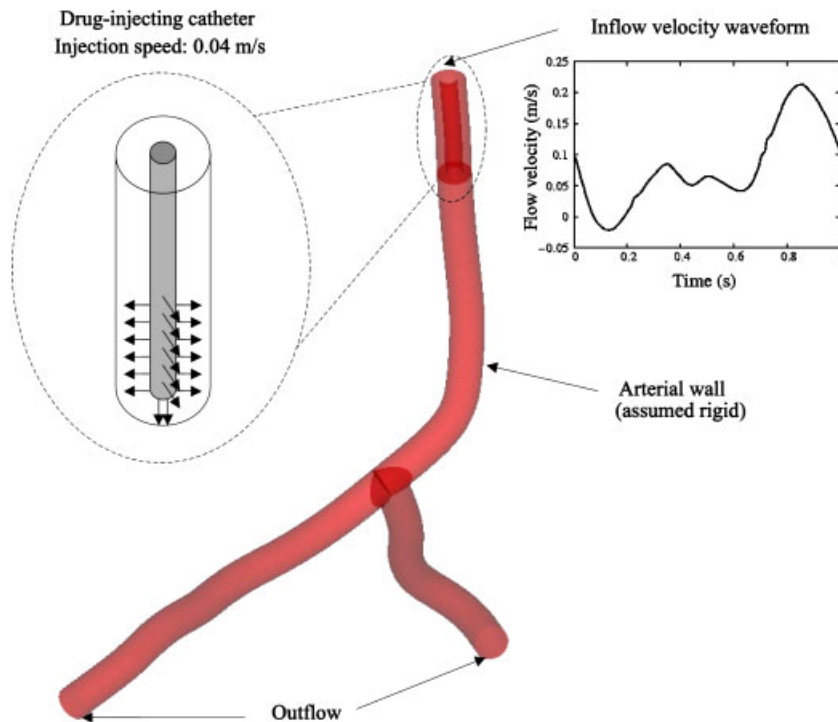

Figure 7. Patient-specific modelling of drug delivery in coronary arteries. Problem set-up.
The inflow data were taken from [26, 27].

the catheter and its tip, as indicated in Figure 7. Prior to the drug being released, a fully periodic flow solution was attained. The drug is released in the beginning of a period and it is injected at a constant velocity thereafter.

The evolution of the drug concentration in the bloodstream is assumed to be governed by a time-dependent advection–diffusion equation with ϕ representing the concentration value. The advection velocity is assumed to come from the solution of the Navier–Stokes equations. It is also assumed that the drug concentration does not influence the flow physics, hence we have a one-way coupling. The drug diffusivity tensor $\boldsymbol{\kappa}$ is assumed to be isotropic and constant with κ taken to be $0.35 \times 10^{-6}\,\mathrm{cm^2/s}$. Boundary conditions for the drug concentration are as follows: on the catheter, where the injection velocity is non-zero, the drug concentration is set to one, while on the rest of the catheter, as well as at the inflow, the drug concentration is set to zero. Arterial walls and outflow boundaries are assigned a homogeneous Neumann boundary condition.

Isogeometric analysis employing quadratic NURBS is used for the spatial discretization. The arterial wall is assumed rigid in the computations, as the focus is placed on the advection–diffusion formulation rather than on the fluid–structure interaction. Future work will entail extending the drug delivery formulation to fluid–structure interaction with a poroelastic arterial wall. Applications of NURBS-based isogeometric analysis to fluid–structure interaction in arterial blood flow, where the arterial wall is assumed deformable, can be found in [11, 28].

A residual-based multiscale method (see e.g. [29–31]), founded on the variational multiscale formulation of the Navier–Stokes equations of incompressible flows (see e.g. [32–37]), is used for the fluid mechanics part. These residual-based methods possess a dual nature: on the one hand, they are bona-fide LES-like turbulence models, and on the other hand, they may be thought of as stabilized methods, such as the SUPG formulation, extended to the nonlinear realm and capable of accurately solving laminar flows. For the scalar advection–diffusion equation we use the $YZ\beta$ discontinuity-capturing formulation with $\beta = 1$. For this case we use a definition of τ that is different from (9) and that is more suitable for complex element geometries

$$\tau = (4/\Delta t^2 + \mathbf{a} \cdot \mathbf{Ga} + 9p^4 \nu^2 \mathbf{G} : \mathbf{G})^{-1/2} \tag{18}$$

where $\mathbf{G}$ is a second-rank metric tensor

$$\mathbf{G} = \left(\frac{\partial \boldsymbol{\xi}}{\partial \mathbf{x}}\right)^{\mathrm{T}} \frac{\partial \boldsymbol{\xi}}{\partial \mathbf{x}} \tag{19}$$

$\partial \boldsymbol{\xi}/\partial \mathbf{x}$ is the inverse Jacobian of the element mapping between the parent and the physical domain, and Δt is the time step.

Remark
Although in the previous section of the paper it was found that high-order, high-continuity NURBS are able to produce sharp interior layers without the aid of discontinuity capturing, the use of high-order NURBS, in their current implementation, is prohibitively expensive for this application. As a result, we used a more economical option, namely NURBS of second order in conjunction with discontinuity capturing.

Figure 8 shows snapshots of the drug concentration in the interior of the coronary artery at $t = 0.2$ and $0.8\,\mathrm{s}$ during four heartbeat cycles. Note that no significant overshoots and undershoots in the solution are present. Also note the quality of the sharp layers, which does not degrade as the scalar is advanced in time for several heartbeat cycles. This is due to the superior robustness
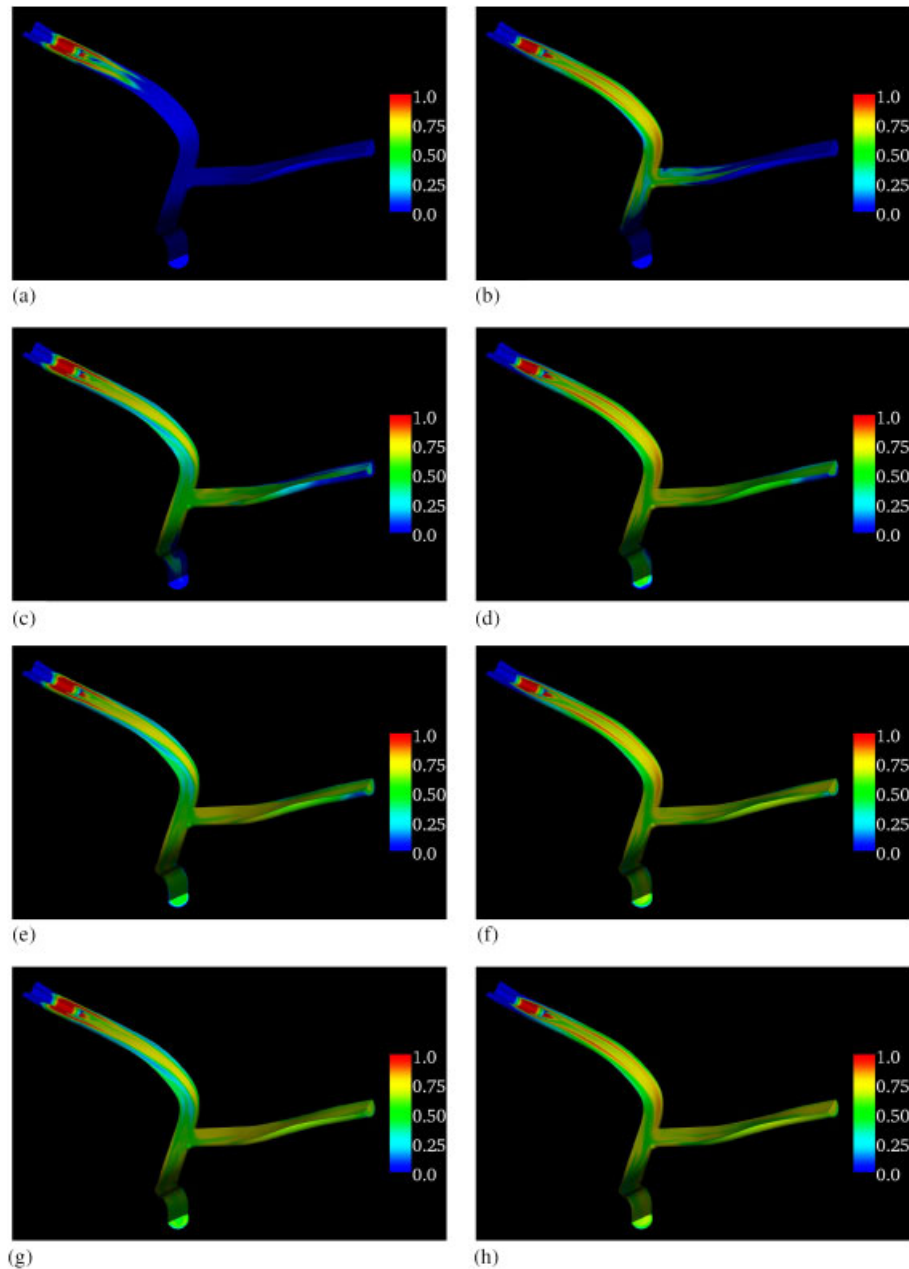
Figure 8. Patient-specific modelling of drug delivery in coronary arteries. Drug concentration in the interior of the arteries at various instants during the simulation: (a) cycle one, $t = 0.2$ s; (b) cycle one, $t = 0.8$ s; (c) cycle two, $t = 0.2$ s; (d) cycle two, $t = 0.8$ s; (e) cycle three, $t = 0.2$ s; (f) cycle three, $t = 0.8$ s; (g) cycle four, $t = 0.2$ s; and (h) cycle four, $t = 0.8$ s.
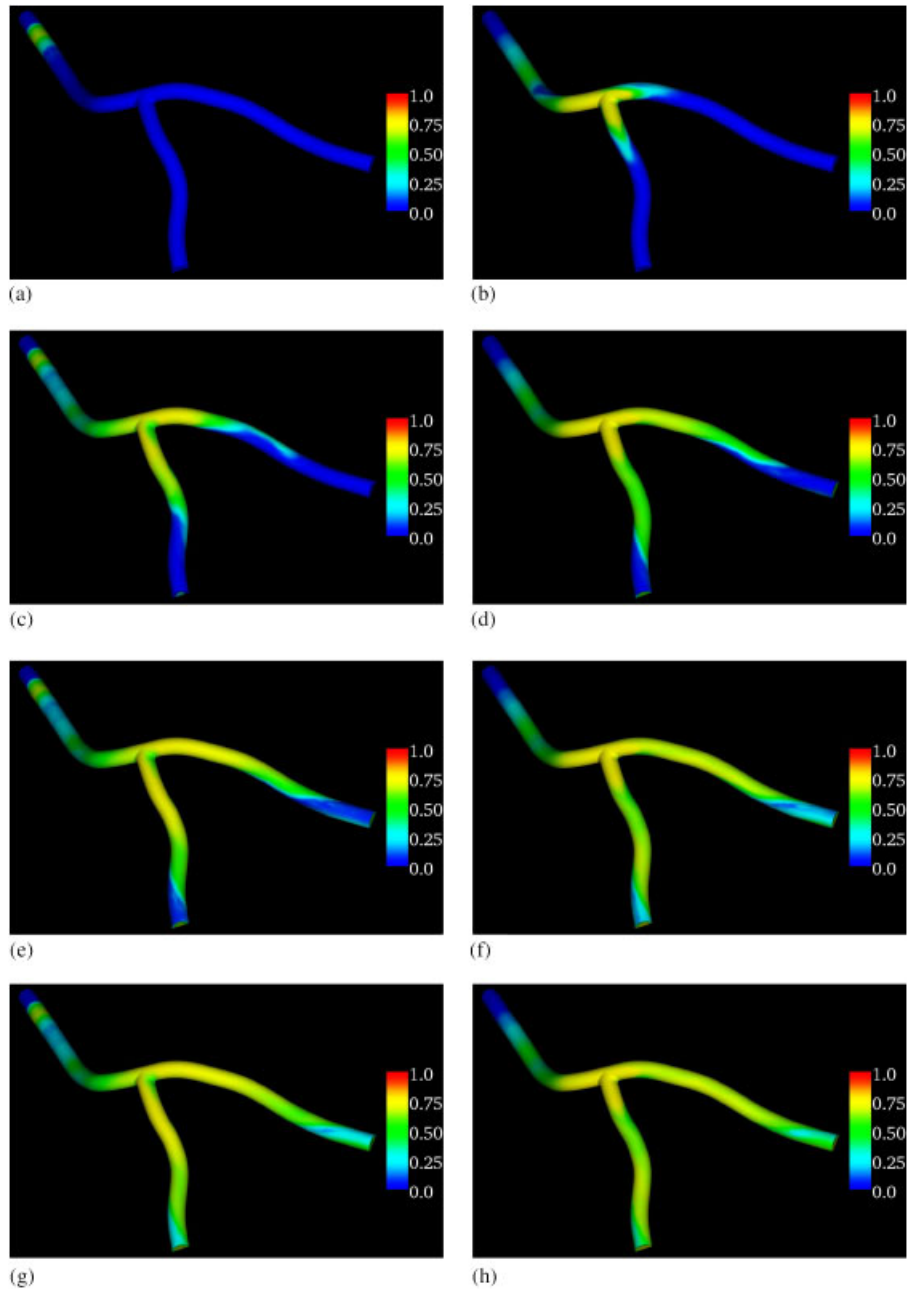
Figure 9. Patient-specific modelling of drug delivery in coronary arteries. Drug concentration at the arterial wall at various instants during the simulation: (a) cycle one, $t = 0.2$ s; (b) cycle one, $t = 0.8$ s; (c) cycle two, $t = 0.2$ s; (d) cycle two, $t = 0.8$ s; (e) cycle three, $t = 0.2$ s; (f) cycle three, $t = 0.8$ s; (g) cycle four, $t = 0.2$ s; and (h) cycle four, $t = 0.8$ s.
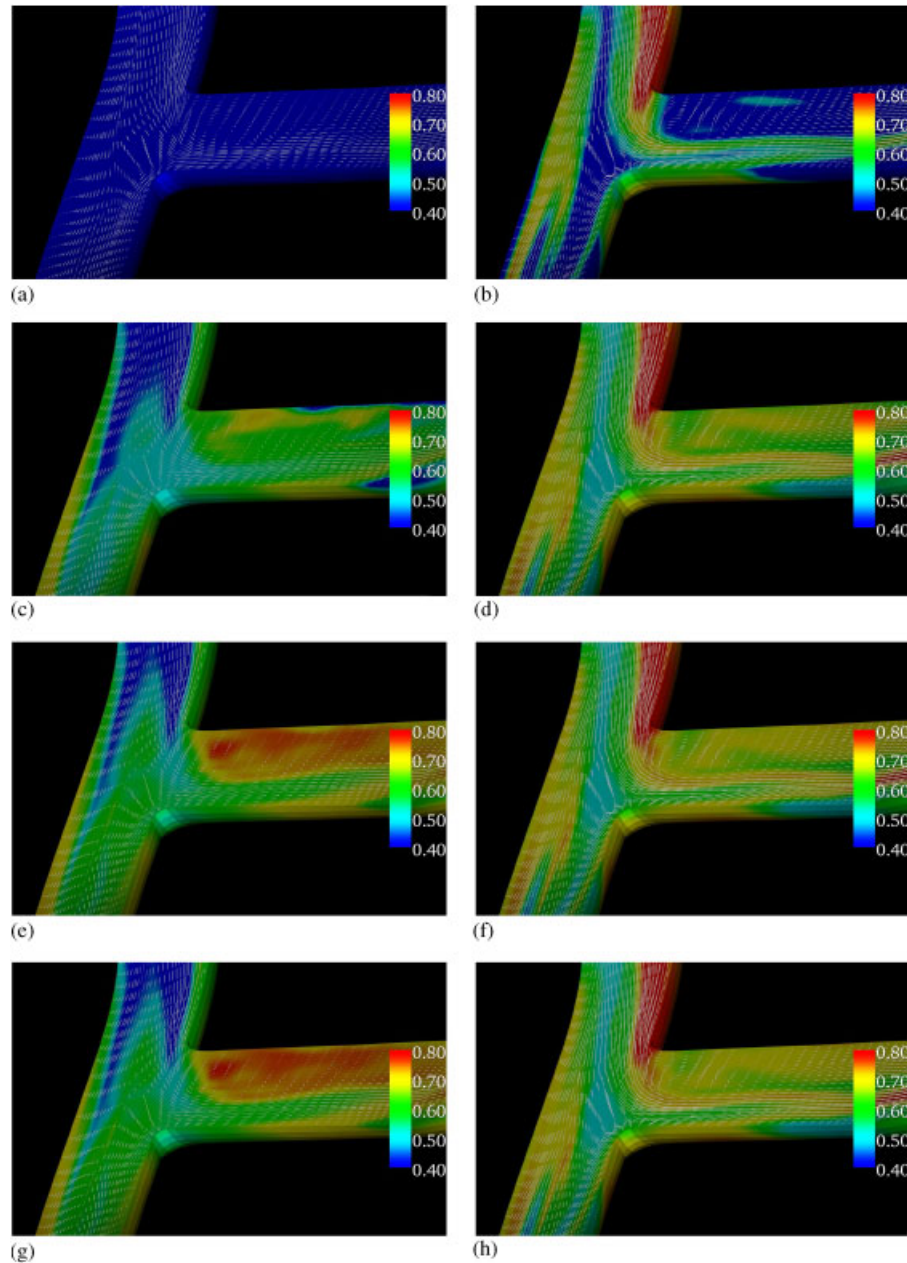
Figure 10. Patient-specific modelling of drug delivery in coronary arteries. Blood flow velocity vectors superimposed on the drug concentration value at the arterial branching. Note the high concentration of drug in the recirculation zone. Also note that the differences between the third and fourth heartbeat cycles are minor, suggesting that a nearly time-periodic solution is achieved: (a) cycle one, $t = 0.2$ s; (b) cycle one, $t = 0.8$ s; (c) cycle two, $t = 0.2$ s; (d) cycle two, $t = 0.8$ s; (e) cycle three, $t = 0.2$ s; (f) cycle three, $t = 0.8$ s; (g) cycle four, $t = 0.2$ s; and (h) cycle four, $t = 0.8$ s.

of the $YZ\beta$ discontinuity-capturing scheme. The longer the drug is injected into the blood stream, the more it is deposited on the arterial walls. This effect can be seen in Figure 9. Also note that at $t = 0.2$ s, at which time the inflow waveform is approximately zero (see insert in Figure 7), most of the inflow volume comes from the catheter, which results in increased drug concentration at the wall immediately near the catheter, since the drug is injected normal to the stream-wise direction. On the other hand, at $t = 0.8$ s, most of the flow goes in the stream-wise direction, carrying the drug with it and depositing very little on the wall adjacent to the catheter. Figures 8 and 9 clearly demonstrate this feature.

In all cases, the highest drug concentration at the wall is achieved in the region where the artery bifurcates. It is also at the bifurcation that the flow is mostly three dimensional, containing complex structures, such as swirling and recirculation. This indicates that the drug is more likely to be deposited on the artery wall where the flow is most unsteady. A detailed view of the bifurcation area is shown in Figure 10, from which we observe that by the fourth heart cycle both the fluid and the drug solutions become nearly time-periodic.

5. CONCLUSIONS

We have extended the $YZ\beta$ formulation to the time-dependent, scalar advection–diffusion equation and recast it in a residual-based form. Using a simple test case we demonstrated that the inclusion of the time-dependent part of the differential operator in the definition of Z is important in order to produce sharp interior layers without excessive overshooting and undershooting. We also found that the residual-based formulation exhibits weaker dependence on the sharpness parameter β than its advective counterpart. In the case of B-splines of high order and high continuity, the SUPG formulation without the aid of discontinuity capturing produced very good interior layers.

We have successfully applied the $YZ\beta$ formulation to patient-specific modelling of drug delivery in coronary arteries. We have observed that the formulation is capable of preserving sharp features of the solution for several heartbeat cycles without degrading quality, and exhibiting a high level of robustness necessary for real-world applications. A more extensive exploration of drug delivery in arteries is in progress.

While stabilized methods may be derived on the basis of the variational multiscale methodology, discontinuity capturing is an *ad hoc* technique. Nevertheless, it is a widely used technology that enables a practitioner to successfully tackle real-world applications. We believe that the multiscale framework with a proper set of optimality conditions is the right underlying theoretical structure that may more naturally lead to discontinuity-capturing formulations. This conjecture is intriguing and warrants further investigation.

REFERENCES

1. Brooks AN, Hughes TJR. Streamline upwind/Petrov–Galerkin formulations for convection dominated flows with particular emphasis on the incompressible Navier–Stokes equations. *Computer Methods in Applied Mechanics and Engineering* 1982; **32**:199–259.
2. Tezduyar TE. Finite element methods for fluid dynamics with moving boundaries and interfaces. In *Encyclopedia of Computational Mechanics*, *Vol. 3*: *Fluids*, Chapter 17, Stein E, De Borst R, Hughes TJR (eds). Wiley: New York, 2004.
3. Tezduyar TE, Senga M. Stabilization and shockcapturing parameters in SUPG formulation of compressible flows. *Computer Methods in Applied Mechanics and Engineering* 2006; **195**:1621–1632.
4. Tezduyar TE, Senga M. SUPG finite element computation of inviscid supersonic flows with *YZβ* shock-capturing. *Computers and Fluids* 2007; **36**:147–159.
5. Tezduyar TE, Senga M, Vicker D. Computation of inviscid supersonic flows around cylinders and spheres with the SUPG formulation and *YZβ* shock-capturing. *Computational Mechanics* 2006; **38**:469–481.
6. Bazilevs Y, Beirao da Veiga L, Cottrell JA, Hughes TJR, Sangalli G. Isogeometric analysis: approximation, stability and error estimates for *h*-refined meshes. *Mathematical Models and Methods in Applied Sciences* 2006; **16**:1031–1090.
7. Cottrell JA, Reali A, Bazilevs Y, Hughes TJR. Isogeometric analysis of structural vibrations. *Computer Methods in Applied Mechanics and Engineering* 2006; **195**:5257–5297.
8. Hughes TJR, Cottrell JA, Bazilevs Y. Isogeometric analysis: CAD, finite elements, NURBS, exact geometry, and mesh refinement. *Computer Methods in Applied Mechanics and Engineering* 2005; **194**:4135–4195.
9. Chung J, Hulbert GM. A time integration algorithm for structural dynamics with improved numerical dissipation: the generalized-α method. *Journal of Applied Mechanics* 1993; **60**:371–375.
10. Jansen KE, Whiting CH, Hulbert GM. A generalized-α method for integrating the filtered Navier–Stokes equations with a stabilized finite element method. *Computer Methods in Applied Mechanics and Engineering* 1999; **190**: 305–319.
11. Zhang Y, Bazilevs Y, Goswami S, Bajaj C, Hughes TJR. Patient-specific vascular NURBS modeling for isogeometric analysis of blood flow. *Computer Methods in Applied Mechanics and Engineering* 2006, submitted for publication.
12. Akin JE, Tezduyar TE. Calculation of the advective limit of the SUPG stabilization parameter for linear and higher-order elements. *Computer Methods in Applied Mechanics and Engineering* 2004; **193**:1909–1922.
13. Bischoff M, Bletzinger K-U. Improving stability and accuracy of Reissner–Mindlin plate finite elements via algebraic subgrid scale stabilization. *Computer Methods in Applied Mechanics and Engineering* 2004; **193**: 1491–1516.
14. Bochev PB, Gunzburger MD, Shadid JN. On inf–sup stabilized finite element methods for transient problems. *Computer Methods in Applied Mechanics and Engineering* 2004; **193**:1471–1489.
15. Burman E, Hansbo P. Edge stabilization for Galerkin approximations of convection–diffusion–reaction problems. *Computer Methods in Applied Mechanics and Engineering* 2004; **193**:1437–1453.
16. Codina R, Soto O. Approximation of the incompressible Navier–Stokes equations using orthogonal subscale stabilization and pressure segregation on anisotropic finite element meshes. *Computer Methods in Applied Mechanics and Engineering* 2004; **193**:1403–1419.
17. Coutinho ALGA, Diaz CM, Alves JLD, Landau L, Loula AFD, Malta SMC, Castro RGS, Garcia ELM. Stabilized methods and post-processing techniques for miscible displacements. *Computer Methods in Applied Mechanics and Engineering* 2004; **193**:1421–1436.
18. Gravemeier V, Wall WA, Ramm E. A three-level finite element method for the instationary incompressible Navier–Stokes equations. *Computer Methods in Applied Mechanics and Engineering* 2004; **193**:1323–1366.
19. Harari I. Stability of semidiscrete formulations for parabolic problems at small time steps. *Computer Methods in Applied Mechanics and Engineering* 2004; **193**:1491–1516.
20. Hauke G, Valiño L. Computing reactive flows with a field Monte Carlo formulation and multi-scale methods. *Computer Methods in Applied Mechanics and Engineering* 2004; **193**:1455–1470.
21. Koobus B, Farhat C. A variational multiscale method for the large eddy simulation of compressible turbulent flows on unstructured meshes—application to vortex shedding. *Computer Methods in Applied Mechanics and Engineering* 2004; **193**:1367–1383.
22. Masud A, Khurram RA. A multiscale/stabilized finite element method for the advection–diffusion equation. *Computer Methods in Applied Mechanics and Engineering* 2004; **193**:1997–2018.

23. Tezduyar TE, Sathe S. Enhanced-discretization space–time technique (EDSTT). *Computer Methods in Applied Mechanics and Engineering* 2004; **193**:1385–1401.
24. Tezduyar TE. Computation of moving boundaries and interfaces and stabilization parameters. *International Journal for Numerical Methods in Fluids* 2003; **43**:555–575.
25. Tezduyar TE. Finite elements in fluids: stabilized formulations and moving boundaries and interfaces. *Computers and Fluids* 2007; **36**:191–206.
26. Johnston BM, Johnston PR, Corney S, Kilpatrick D. Non-Newtonian blood flow in human right coronary arteries: transient simulation. *Journal of Biomechanics* 2006; **36**:1116–1128.
27. Matsuo S, Tsuruta M, Hayano M, Immamura Y, Eguchi Y, Tokushima T, Tsuji S. Phasic coronary artery flow velocity determined by Doppler flowmeter catheter in aortic stenosis and aortic regurgitation. *The American Journal of Cardiology* 1988; **62**:917–922.
28. Bazilevs Y, Calo VM, Zhang Y, Hughes TJR. Isogeometric fluid–structure interaction analysis with applications to arterial blood flow. *Computational Mechanics* 2006; **38**:310–322.
29. Bazilevs Y. Isogeometric analysis of turbulence and fluid–structure interaction. *Ph.D. Thesis*, ICES, UT Austin, 2006.
30. Calo VM. Residual-based multiscale turbulence modeling: finite volume simulation of bypass transition. *Ph.D. Thesis*, Department of Civil and Environmental Engineering, Stanford University, Stanford, 2004.
31. Hughes TJR, Calo VM, Scovazzi G. Variational and multiscale methods in turbulence. In *Proceedings of the XXI International Congress of Theoretical and Applied Mechanics* (*IUTAM*), Gutkowski W, Kowalewski TA (eds). Kluwer: Dordrecht, 2004.
32. Holmen J, Hughes TJR, Oberai AA, Wells GN. Sensitivity of the scale partition for variational multiscale LES of channel flow. *Physics of Fluids* 2004; **16**(3):824–827.
33. Hughes TJR, Mazzei L, Jansen KE. Large-eddy simulation and the variational multiscale method. *Computing and Visualization in Science* 2000; **3**:47–59.
34. Hughes TJR, Mazzei L, Oberai AA, Wray AA. The multiscale formulation of large eddy simulation: decay of homogeneous isotropic turbulence. *Physics of Fluids* 2001; **13**(2):505–512.
35. Hughes TJR, Oberai AA, Mazzei L. Large-eddy simulation of turbulent channel flows by the variational multiscale method. *Physics of Fluids* 2001; **13**(6):1784–1799.
36. Hughes TJR, Scovazzi G, Franca LP. Multiscale and stabilized methods. In *Encyclopedia of Computational Mechanics*, *Vol. 3*, *Computational Fluid Dynamics*, Chapter 2, Stein E, De Borst R, Hughes TJR (eds). Wiley: New York, 2004.
37. Hughes TJR, Wells GN, Wray AA. Energy transfers and spectral eddy viscosity of homogeneous isotropic turbulence: comparison of dynamic Smagorinsky and multiscale models over a range of discretizations. *Physics of Fluids* 2004; **16**:4044–4052.